LAJSBA
LATIN AMERICAN JOURNAL OF SEDIMENTOLOGY AND BASIN ANALYSIS | VOLUME 31 (2) 2024, 103-118

HYDROGEOMORPHOLOGICAL CHANGES AND THE EROSION-DEPOSITION IMPACT IN THE SAN FRANCISCO RIVER BASIN, NORTHWEST ARGENTINA: A MULTIDECADAL ANALYSIS

María A. Isuani[1], Sergio M. Georgieff [2], María S. Bustos[3]*

[1] CONICET NOA SUR. Miguel Lillo 205, San Miguel de Tucumán, Tucumán, Argentina.
[2] Facultad de Ciencias Naturales e IML, UNT, CONICET. Miguel Lillo 205, San Miguel de Tucumán, Tucumán, Argentina.
[3] Instituto de Ecosistemas de Aguas Continentales (IEAC), Fundación Miguel Lillo. Miguel Lillo 251, San Miguel de Tucumán, Tucumán, Argentina.
*Corresponding author: antonella.isuani@gmail.com

ARTICLE INFO

Article history
Received February 2, 2024
Accepted June 28, 2024
Available online July 18, 2024

Handling Editor
Giorgio Basilici

Keywords
River basin
Flow
Solids Transport
Anthropic activity
Northwest Argentina

ABSTRACT

Modifications of wetland and forest areas are studied, in particular, to establish to what extent they are sensitive to natural changes (*e.g.*, increased precipitation and/or temperature) in addition to human activities (*e.g.*, advancing agricultural frontier, deforestation, channelizations). The San Francisco River Basin (SFRB; 1,789 km^2) is located in the Northwest of Argentina in the Geological Province of Nortwestern Pampean Ranges (*Sierras Pampeanas Noroccidentales*), between 27°40'S and 28°25'S, and 65°15'W and 65°45'W). In recent decades, agricultural development and management in the middle and lower SFRB generated rural channelizations (the largest of 10 km at the basin outlet between 2005-2015), drainage of wetland forests, deforestation of native dry forest since 1995 and changes in land use. In addition, a 200 mm increase in mean annual rainfall since 1972 and an increase in extreme hydrological events, are registered. These modifications produced changes in local base level, erosive processes of retreat and the development of new river channels from upstream, increasing flow velocities, flow rates, and sediment discharge. The intensified erosive processes resulted in four new river courses in the middle and lower basin, incorporating the SFRB into the Marapa river basin, changing from arheic to endorheic behaviour, and generating the contribution of liquid and solid flows to the system of which it is now a part. The aim of this study is to examine the development of the new hydrographic network within the SFRB between 1990 and 2018 and to calculate the solid and liquid discharges generated by the new network. The hydrographic network formed by the rivers El Abra, Ovanta, San Francisco and Suncho creek, was digitized in the open-source software QGIS 3.18.3 on the basis of the visual interpretation of satellite imagery. The lengths of the rivers were automatically calculated and exported to a spreadsheet to determine the downstream expansion of the river network. Measurements and sampling of water discharge and sediment load were performed monthly in the lower section of the SFRB. The float and cross-section method was used to quantify the flow rates, and the sediment samples were filtered, dried in an oven for 24 h and weighed on a precision balance to obtain the sediment concentration (C in mg/l). The study determined the generation of

102 km of new river channels in a 28 yr period. The hydrographic network had an annual sediment production of 82,138 t/yr and an annual discharge of 21,96 hm^3, contributing to the Marapa river basin and generating an acceleration in the silting of the downstream Río Hondo reservoir. This work provides a basis for management and mitigation of erosion and flooding problems in the area.

INTRODUCTION

The forested wetlands (*bañados arbolados*) and native forests in the middle and lower subtropical watersheds are considered stable environments and their sedimentary processes have received little attention in terms of the effects of other natural changes (*e.g.*, increased precipitation and/or temperature) and human activities (*e.g.*, advancing agricultural frontier, stream regulations, and channelizations).

Since the last decade of 20th Century, the watersheds of northern and central Argentina show changes associated with extreme hydrological events (floods and droughts), increases in mean annual precipitation and land use changes that have unbalanced the basins, enhanced erosive processes and generated new fluvial streams (Contreras *et al.*, 2012; Eremchuk, 2016; Buono *et al.*, 2018). Anthropogenic activities record the advance of the extensive agriculture and loss of the forest masses: 1,757,600 ha between 2000 and 2007, and 1,912,016 ha between 2007 and 2016 (Volante *et al.*, 2012; Azcuy Ameghino and Ortega, 2010-12; CIST, 2017).

In the southern of Tucuman and eastern of Catamarca provinces, streams and irrigation surpluses of the San Francisco River Basin (SFRB; Fig. 1a), used to reach forested wetlands and native forests as low velocity laminar flows, favouring infiltration and deposition processes. Rural channelizations (the major one of 10 km channelization at the outlet of the catchment between 2005–2011), drainage of wetland forests, deforestation of native dry forest since 1995 (CIST, 2017), changes in land use (Díaz and Gaspari, 2017), the increase of 200 mm in average annual precipitation since 1972 (Eremchuk *et al.*, 2016; Bazzano, 2019), and extreme hydrological events (*e.g.*, March 25th and April 2nd, 2017; La Gaceta, 2017) produced modifications in the local base level, backward erosional processes and development of new fluvial channels from upstream, increasing flow velocities, flow rates, and sediment discharge. Piping, sapping, and the formation of gullies in the floodplain (CIST, 2017) were contemporary processes. The new scenario transformed the middle and lower parts of the basin (CEEH, 2018) generating the development of four new river courses in the last three decades.

This transformation of the watershed altered the drainage network systems and natural hydrographic dynamics modifying the cycle of infiltration and evapotranspiration in wetland forests and native forests. The new fluvial system is formed by permanent streams and rivers (endorheic system) instead of the previous ephemeral streams (arheic system). The modifications of hydrographic dynamics by natural changes and human intervention were recorded among others by Contreras (2012) and Zilio *et al.* (2022) in San Luis, Argentina, studying the processes of canyon and stream formation in a semiarid catchment. Lu *et al.* (2021) discussed watershed reorganization and endorheic-exorheic transition in Chinese lake basins.

The enlargement of the drainage network of the SFRB and new flows discharge (water and sediments) firstly deposited large splay lobes along the margins in the lower basin (April 2017) and induced around 2,900 m of downstream displacement of the outlet (and confluence zone with Marapa river; Fig. 2); secondly, the frequency of flooding increased (La Gaceta, 2017; CEEH, 2018; El Esquiú, 2023); and thirdly, produced an acceleration of the Río Hondo reservoir clogging. An example of this was a peak discharge of 30 hm^3 of sediment (CEEH, 2018) at the mouth on the Marapa River in only one extreme event occurred between March 31 and April 1, 2017 (CIST, 2017; CEEH, 2018).

The main goals of the present study are 1) to analyse the development of new streams in the SFRB between 1990 and 2018, 2) to assess the lengths and widths of these new channel-beds, 3) to calculate the annual flow rate (AFR), average monthly flow rate (AMF), total annual sediment load (TAL), and average monthly sediment load (AML) measuring water discharge and collecting sediment load samples, monthly, from May 2020 to April 2021, and finally, 4) to relate the generation of new streams to environmental changes.

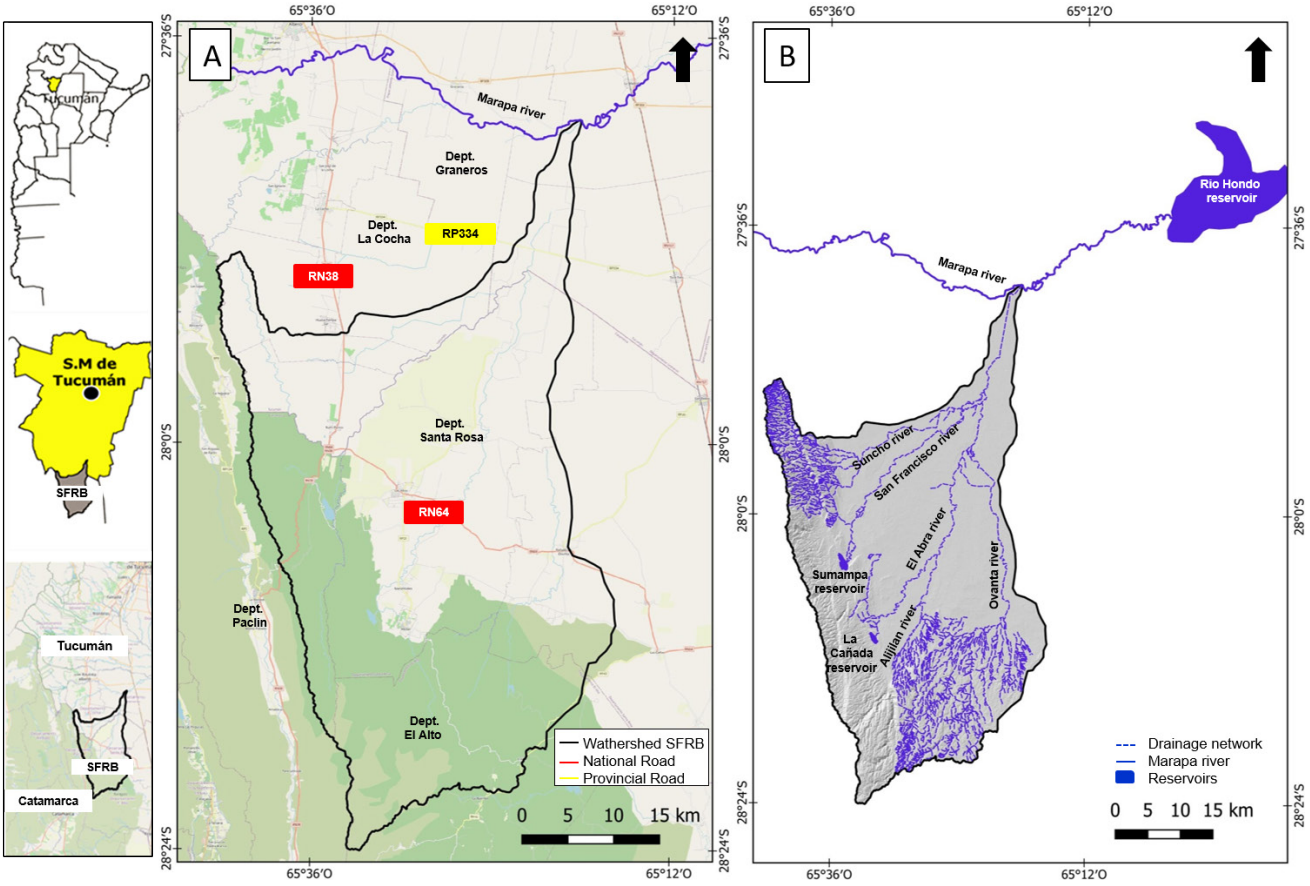

Figure 1. a) Location of the study area. **b)** Draining network of the San Francisco River Basin, Marapa river and reservoirs.

GEOLOGICAL AND HYDROLOGICAL FRAMEWORK

The SFRB (1,789 km^2; located between 27°40'S and 28°25'S, and 65°15'W and 65°45'W; Fig. 1a) covers diverse landscapes, including mountainous regions to the western and southern areas (Ambato and Ancasti ranges), with steep slopes reaching up to 53% and an altitude ranging from 600 to 2,083 m above sea level, generating orographic rainfall in summer. The headwaters and two reservoirs, Sumampa and La Cañada, built for irrigation, are located in this part of the basin (Fig. 1b). On the eastern side, there are flat plains with gentler slopes, typically around and less than 5%, and an altitude range between 600 and 300 m above sea level.

Precambrian – lower Paleozoic rocks are the main component of the mountain ranges that limit the basin, corresponding to a mainly faulted and tilted crystalline basement formed by metamorphic rocks of the Ancasti Formation (Aceñolaza and Toselli, 1977, 1981; Aceñolaza *et al.*, 1983), La Cébila Formation (González Bonorino, 1950; Nullo, 1981), and El Portezuelo Formation (Aceñolaza and Toselli, 1981; Aceñolaza *et al.*, 1983), and post-tectonic plutonic rocks comprising numerous intrusive bodies (*e.g.*, San Ignacio-Los Pinos, El Manchao, Ambato). The Miocene to upper Pliocene continental clastic rocks belonging to the Aconquija, Guasayan, Las Cañas, and Choya formations (Battaglia, 1982; Dal Molin *et al.*, 2003) crop out in the piedmont of main ranges overlying the crystalline basement in discordance. The oldest Pleistocene rocks consist of fanglomerates, sandstones, and siltstones deposited overlaying the Neogene deposits. The modern sedimentary deposits are mainly composed of loess and fluvial gravels and sands (Blasco *et al.*, 1994).

The predominant soils show high erodibility enhance laminar and linear processes in the lower areas of the basin (CEEH, 2018). In the mountain areas the dominant soils belong to the orders Entisols (lithic Ustorthents) and Inceptisols (humic Dystrusteps typic). The Mollisol order predominates in the pedemontane sectors (typical Argiustols) and alluvial plains (typical Haplustolls, fluvial Haplustolls,

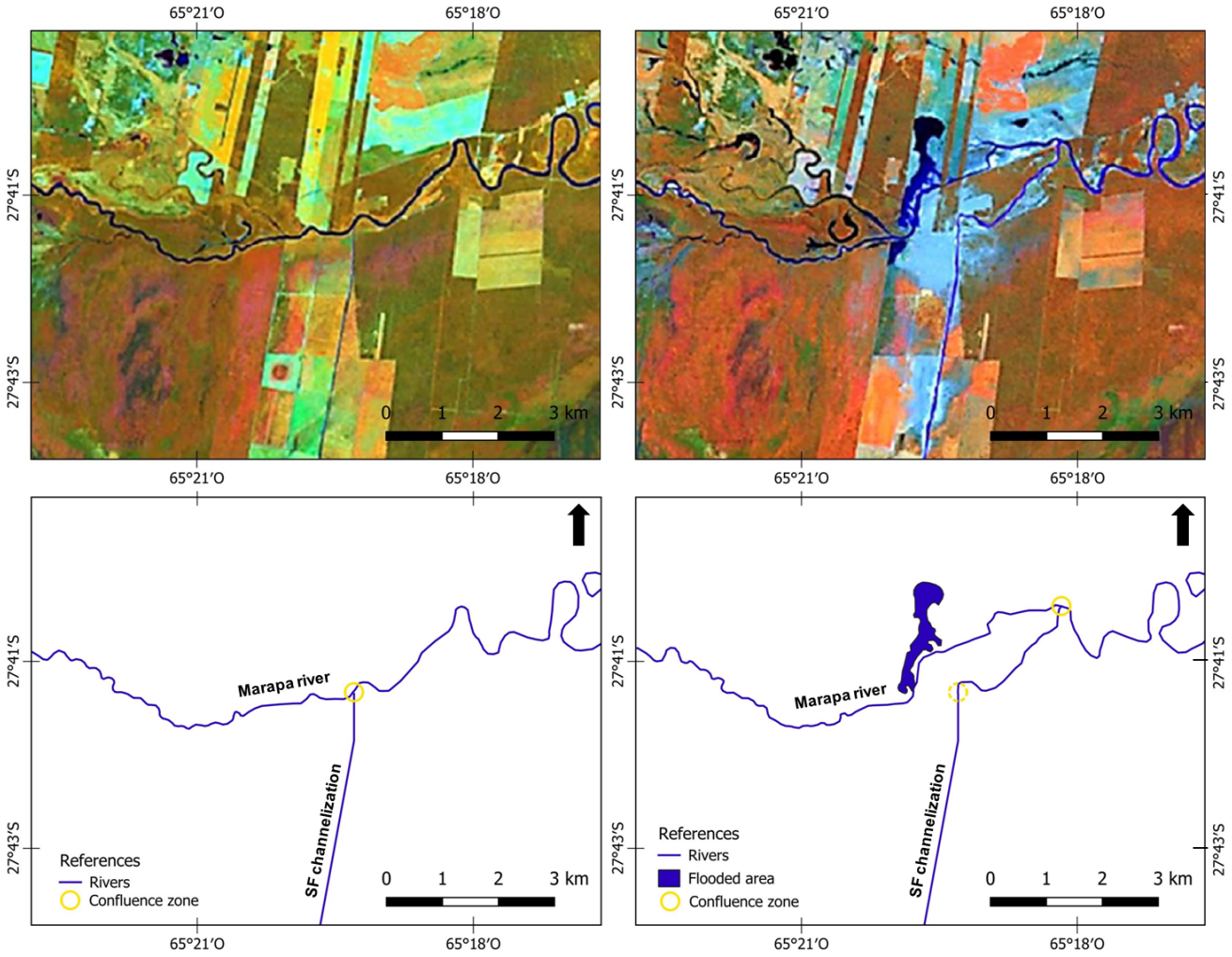

Figure 2. Landsat 8 images before and after extreme flood occurred between March 31st and April 1st, 2017. The blue light area in the confluence zone corresponds to sandy splays (see Fig. 8d) deposited during the flood. Left (sketch and image date: 03-28-2017): San Francisco and Marapa rivers confluence zone and river patterns before the flood, note the location of San Francisco (SF) channelization outlet. Right (sketch and image date: 04-19-2017): new confluence zone location and channel patterns after the flood. The confluence zone shifted about 2,900 m toward downstream (see the text for details).

and udic Haplustolls), while the sectors with fluvial influence (runoff channels, fluvial terraces and flood plains) are dominated by Entisols (typical Udifluvents and Ustifluvents).

The primary flow direction within the SFRB region is from southwest to northeast. Until 2016, the drainage network of this region was intermittent and non-permanent. The main stream is the San Francisco River, which originates in the Cumbre Potrerillos (Paclín Dept, Fig. 1a). It flows in a north-northwest to south-southeast direction until it reaches the vicinity of the town La Viña, where it undergoes a significant change in gradient and then turns northeastward towards the alluvial plain. Before joining the Marapa River in the Graneros Department of Tucumán, the San Francisco River receives inputs from several other rivers, including El Abra or Capellanía, Alijilan and Ovanta rivers from the Ancasti Mountain Range, as well as the Suncho River from the eastern slope of the Cumbre de Potrerillos, which is part of the Sierra de Ambato (Fig. 1b). The average flow of the rivers is strongly influenced by the seasonal rainfalls, with the highest discharge values typically occurring during the spring-summer, from October to March, and the lowest discharge occurring during the dry season from June to September.

The SFRB is situated within a transition area between the Chaco Serrano ecoregion to the west and undergoes a transitional shift towards the Semiarid Chaco to east (Mendoza and González,

2011). Predominant Köppen climate type is Bsk/Bsh according to Mendoza and González (2011). The annual precipitation varies between 500 and 1000 mm, and the average yearly temperatures typically range from 12°C to 22°C (Mendoza and González, 2011; Bazzano, 2019). The western area of the SFRB receives the maximum rainfalls, with the hilly terrain acting as an orographic barrier that intercepts wet winds coming from the Atlantic Ocean (Torrella and Adámoli, 2005).

MATERIALS AND METHODS

To analyze the newly formed fluvial channels, a digitization of the hydrographic network was accomplished using Qgis 3.18.3 open-source software and satellite images. LANDSAT 5 TM images of 1990, 2000, and 2010, and LANDSAT 8 OLI images from 2018, all with a spatial resolution of 30 x 30 m were used as a database. Before visually digitizing the network for different years, we calibrated the images using the Semi-Automatic Classification Plugin (SCP). To cover the entire study area, we combined and cropped scenes based on the vector boundary of the basin. To aid in the visual interpretation of the network, we applied RGB combinations, specifically 6-5-4 for Landsat 8 and 5-4-3 for Landsat 5.

After the network was digitally mapped, the lengths of the riverbeds for the San Francisco, El Abra, Ovanta, and Suncho rivers were automatically calculated for each year. The resulting data was exported to a spreadsheet to determine the length (in kilometres) of the new riverbeds.

In addition, the increase in width of the channels was quantified at three points of the network (Fig. 3a): point 1 (27°46'58.41"S, 65°20'31.25"W), located on the El Abra river upstream of the confluence with the San Francisco river; point 2 (27°48'34.23"S, 65°21'11.67"W), located on the San Francisco river at the junction

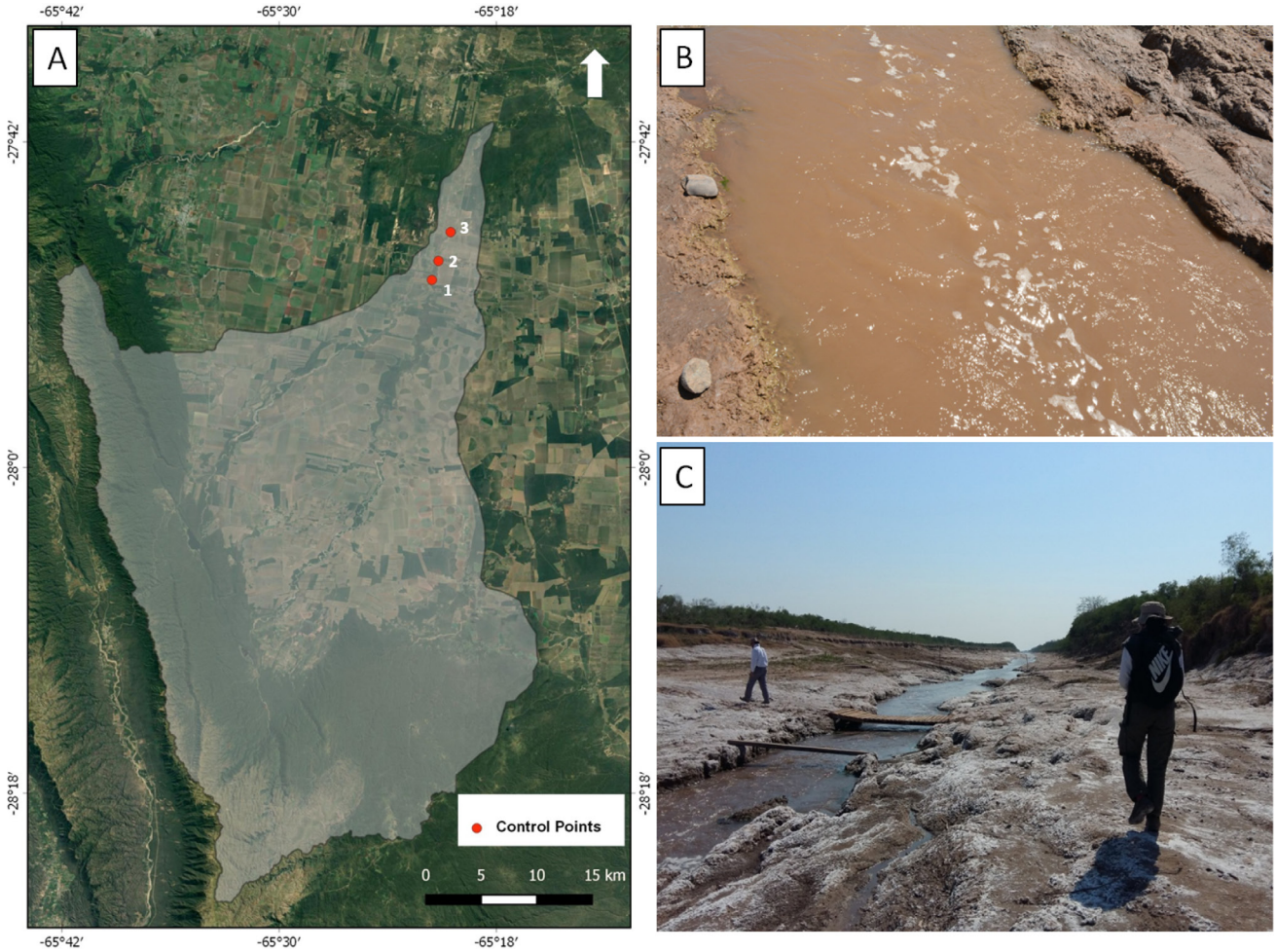

Figure 3. a) Control points in the width increase analysis. **b)** Channelization of the San Francisco River in the month of February 2021 (flow and solid loads sampling area). **c)** Water discharge and sediment load in the channelization of the SFRB.

with provincial route 334 (at this point the river already carries the flow and sediment load of all the tributaries of the network), and point 3 (27°49'37.34"S, 65°21'33.38"W) located upstream of the beginning of the 10 km long channelization that leads the river network into the Marapa river. This last analysis was carried out on Google Earth (TM) temporal series of images for the years 2005, 2016 and 2018/19, using previously downloaded Landsat images as support.

Measurements of sediment and water discharge in the new fluvial course were performed monthly between May 2020 and April 2021 in the lower SFRB (El Zapallar: 27°45'45"S, 65°20'2.22"W; Fig. 3b and 3c). The selected site collects the total streamflow of the basin. These *in situ* measurements were the first recorded for the SFRB.

The quantification of flow rates was conducted using the float and cross-section method. Data on surface velocity were recorded and subsequently adjusted by a factor of 0.8 to determine the average velocity of the water column. Additionally, depth measurements were taken at consistent intervals across the entire width of the channel to calculate the cross-sectional area at the sampling point. The flow rate at the time of sampling (IFR in m^3/s) was calculated using eq. (1):

$$IFR = Vcw \times Ats \quad (1)$$

Where Vcw represents the water column velocity and Ats is the cross-sectional area. To calculate the monthly flow rates (MFR in hm^3/month), eq. (2) was applied:

$$MFR = (IFR \times 86{,}400 \times Dm) \div 1{,}000{,}000 \quad (2)$$

Where the value 86400 is employed to determine the daily discharge in the section, and Dm corresponds to the number of days in the respective month. Finally, the annual flow rate (AFR in hm^3/yrs) for the SFRB during the 2020/2021 period was determined by eq. (3):

$$AFR = \sum_{1}^{12} MFR \quad (3)$$

Samples of sediment from both the riverbed and the suspended sediment were collected using an instantaneous sediment sampler with a capacity of 1 l. The analyzed section had a maximum width of 3 m and a maximum depth of 0.73 m. The maximum depth measured in the transverse profile during each sampling date was selected as a reference for sediment sampling. Suspended sediment was sampled at a depth equivalent to 1/3 of the maximum depth, while sediment from the riverbed was collected directly from the river bottom, where bed irregularities were minimal or negligible. In both cases, before sealing the sampler inlet and outlet, the water flow was allowed to stabilise for 60 seconds. Water samples containing sediment were carefully packaged and labelled in containers for subsequent laboratory analysis. Sediment samples were filtered through previously weighed N°4 filter paper. The material retained in the filters was dried in an oven for 24 h and weighed on a precision balance. The sediment concentration (C in mg/l) was obtained by eq. (4):

$$C = (W_{f+s} - W_f) \div V \quad (4)$$

Where W_{f+s} is the sum of filter weight and retained sediment, W_f is the filter weight and V is the sample volume for both suspended (C_s) bandbackground (C_b) samples (Basile, 2018).

To determine the monthly bed and suspended load (MBL and MSL, in t/month), we considered the previously calculated monthly flow rates and the concentration of each type of sediment (C_s and C_b). The calculation was carried out using eq. (5) and eq. (6):

$$MBL = MFR \times C_b \quad (5)$$

$$MSL = MFR \times C_s \quad (6)$$

The total monthly load (TML in t/month) was obtained by eq. (7):

$$TML = MBL + MSL \quad (7)$$

By summing up the monthly loads, the annual bed load (ABL in t/yr) and annual suspended load (ASL in t/yr) were estimated by eq. (8) and eq. (9):

$$ABL = \sum_{1}^{12} MBL \quad (8)$$

$$ASL = \sum_{1}^{12} MSL \quad (9)$$

The total annual load (TAL in t/yr) was determined by eq. (10):

$$TAL = ABL + ASL \quad (10)$$

The average monthly load (AML in t/month) of the SFRB was obtained as eq. (11):

$$AML = TAL \div 12 \quad (11)$$

RESULTS

The evolution of the drainage network of SFRB is shown in Figure 4. Over the 28 yrs period covered in this study, visual analysis and digitization of stream network reveal the development of 102 km of new river channels in the lower SFRB (Table 1).

Rivers/Years	1990	2000	2010	2018	New km
San Francisco	20	37	43	58	38
El Abra	40	43	58	58	18
Suncho	5	21	26	26	21
Ovanta	17	19	21	42	25
Total	82	120	148	184	102

Table 1. Length of the main watercourses of the basin in the years analyzed and extent of the newly developed network.

At the beginning in the 90's (Fig. 4a), the streams drained to the lower areas where water infiltrated or accumulated (arheic system) feeding a vast area of forested wetlands. The data shown in Table 1 reveals that the longest stream at that moment was El Abra (40 km), followed in length by the San Francisco (20 km), the Ovanta and Suncho (17 and 5 km, respectively). By the end of the study period, in 2018, 38 km were added to the San Francisco (final length 58 km) and 25 km to the Ovanta (final length 42 km). The enlargement of the Suncho river resulted in 21 new kilometres (final length 26 km) and, finally, El Abra river increased its length by 18 km (final length 58 km). The analysis shows a progressive but constant enlargement of streams resulting in the shift of the original drainage network from an arheic system to an endorheic system, delivering water and sediment to the Marapa river basin.

The analysis of the increase in channels widths at three points of the network, revealed a similar trend of increment over the considered 14 yrs period (from 2005 to 2019; Fig. 5). In site one (Fig. 5a), located at El Abra river, upstream the junction with San Francisco, the channel width increased from 6 m (2005) to 60 m (2016) ending at 97 m (2019). This represents a total increment of 91 m at this site of the network. At the second point (Fig. 5b), downstream from site 1, where the San Francisco river crosses route 334, the channel evolved from a very narrow path of only 6 m width in 2005 to a wide channel of 52 m (2016) and 140 m (in 2019). The last point (Fig. 5c), downstream from point 2, close to the head of the channelization shows also the increasing trend but, particularly in this case, at the beginning (2005) the channel bed is not detectable and only crop farmlands and a built-up area are visible. In 2016, the emergence of the channel was evident as an 80-m-wide meandering path, the latter evolving to a 140-m-wide channel in 2019, the widening of which is concomitant with the destruction of the neighbouring built-up area. Also, the visual analysis of remote sensed images corresponding to the three sites reveals how the surrounding landscape to the sites had changed with an apparent decrement in the area covered by natural forests.

Table 2 shows IFR, MFR and AFR for the sampling period. The greater values were recorded in March'21 (1.43 m^3/s) and April'21 (1.35 m^3/s), towards the end of the wet season in the region. Values decrease along the hydrologic year resulting in the lowest value (0.29 m^3/s) in October'20, at the end of the dry season. The annual flow rate for the basin was 21,96 hm^3 and the average monthly flow was 1.83 hm^3/month.

Regarding sediment measurement, sediment-transport rate for suspended sediment (g/l) is shown in Table 3 together with sediment-transport rate for bed load. In the table, there are also the values corresponding to monthly sediment load (t/month) for suspended and bed load (MSL and MBL) and data representing total annual suspended load (ASL), total annual bed load (ABL) and the Total Annual Load (TAL). The TAL calculated was 82,138 t/yr, corresponding to 27,292.8 t/yr for ABL and 54,845.28 t/yr for the ASL.

The total monthly load (TML) is illustrated in Figure 6; the months of June, March, and April stand out for presenting the highest transported load. The Average Monthly Load (AML) of transported solids is estimated to be 6,845 t/month.

IMPLICATION OF THE NEW DRAINAGE NETWORK

The results reveal a consistent growth in the length of the drainage network from 1990 until its final connection with the Marapa river in 2017, resulting in 102 kilometres of new fluvial courses in 28 years. The changes of the drainage network were driven by two

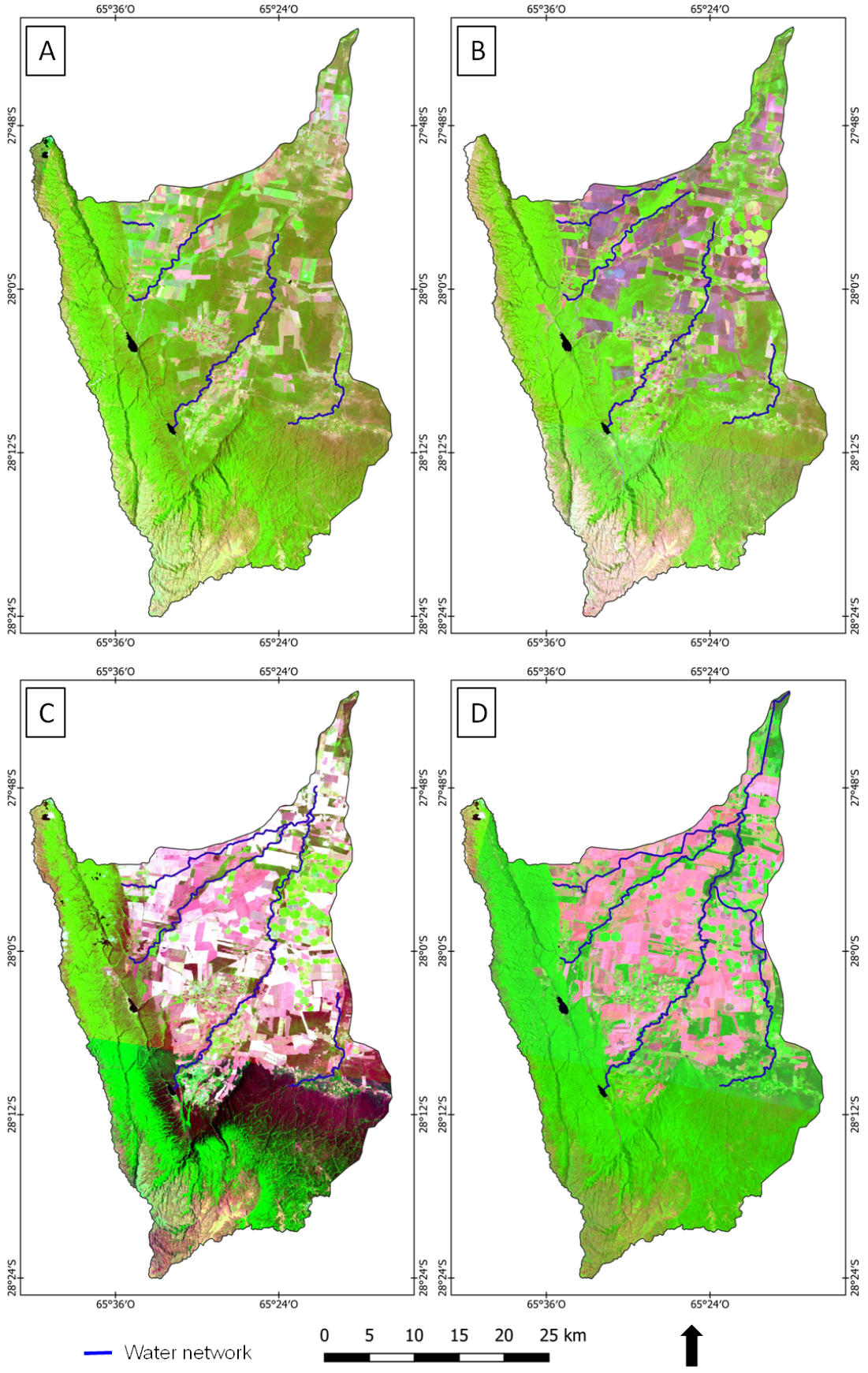

Figure 4. Evolution of the SFRB drainage network. **a)** Extent for the year 1990. **b)** Extent for the year 2000. **c)** Extent for the year 2010. **d)** Extent for the year 2018.

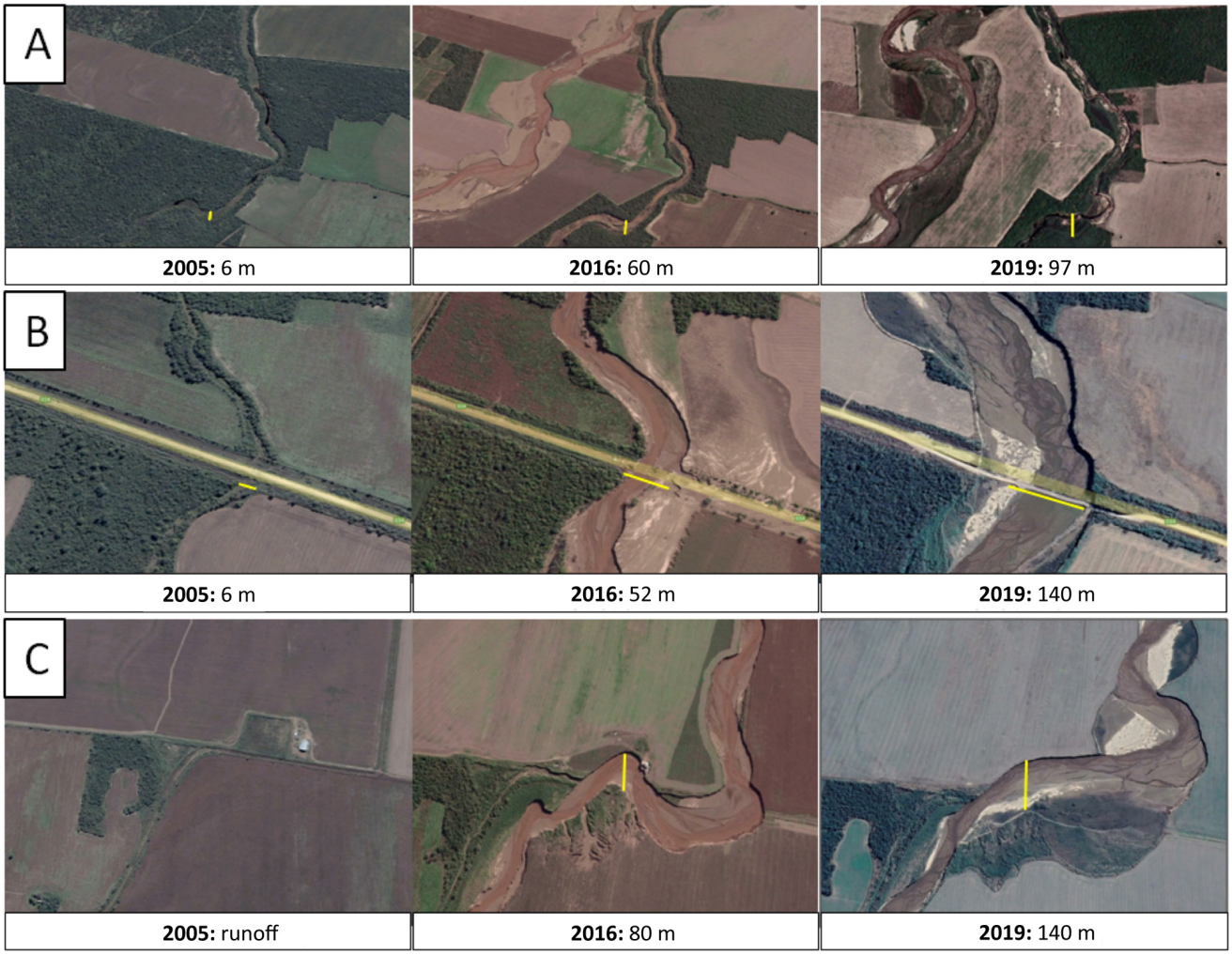

Figure 5. Width increment in main channels. **a)** Point 1 - El Abra river (27°46'58.41"S, 65°20'31.25"O). **b)** Point 2 - San Francisco river (27°48'34.23"S°, 65°21'11.67"O). **c)** Point 3 - San Francisco river - Channelization point (27°49'37.34"S, 65°21'33.38"O).

main principal processes (Fig. 7): 1) sapping and piping in the floodplain (recorded in all rivers of the SFRB) along with the development of gullies in the margins of the rivers, allowing the initiation of small streams; the channels are broad in downstream direction and narrow in upstream direction; 2) base-level control through the formation of new courses by advancing of depositional lobes and floodplain erosion due to base-level drop between rivers (e.g., San Francisco river regarding to El Abra river, and Suncho river regarding to San Francisco river) converted the original arheic system (Fig 4a, 1990) to an endorheic basin feeding the Marapa river (Fig 4d, 2018).

Previous studies (*e.g.*, Bakker *et al.*, 2005; Zheng, 2006; Capolongo *et al.*, 2008; Coe *et al.*, 2011; Pierce *et al.*, 2012) have stated that the transformation of wetlands by agricultural expansion produce channels and tributaries-plain disconnection, stream incision processes, bank erosion, increased water velocities leading to flow variability and intensification of peak discharges.

As of 2017, the new draining system of SFRB is composed by four fluvial basins, which deliver solid and liquid flows to the lower Marapa Basin and Río Hondo reservoir. At the same time, the state of SFRB became permanent and began to supply or at least to transport more than 82,138 t/yr of sediments accompanied by water discharge up to 21.96 hm^3 into the Marapa river. Thus, the drainage area at the confluence of both basins (Marapa and San Francisco rivers; Fig. 2) doubled the original Marapa basin area from 1,759 km^2 (CIST, 2017; Guido *et al.*, 2022) to 3,541 km^2 (when SFRB became a tributary). This way, the modern scenario certainly increases the sedimentation

Month	IFR	MFR
May 20’	0.76	2.04
June 20’	0.8	2.07
July 20’	0.69	1.85
August 20’	0.73	1.96
September 20’	0.61	1.58
October 20’	0.29	0.78
November 20’	0.39	1.01
December 20’	0.54	1.45
January 21’	0.33	0.88
February 21’	0.42	1.02
March 21’	1.43	3.83
Aprill 21’	1.35	3.50
AFR		**21.96**

Table 2. Instantaneous (IFR), monthly (MFR) and anual (AFR) flow records for the sampling period

Month	Cs	Cb	MSL	MBL
May 20’	0.06	0.12	122.14	4.07
June 20’	2.84	134.70	5891.31	4810.50
July 20’	1.34	78.73	2473.49	2424.86
August 20’	1.54	44.73	3001.28	1457.51
September 20’	1.32	90.10	2090.24	2453.53
October 20’	2.61	50.59	2023.40	654.92
November 20’	0.80	36.05	807.39	627.58
December 20’	2.10	6.64	3040.20	159.98
January 21’	0.74	52.78	640.50	765.71
February 21’	2.40	7.61	2443.02	142.65
March 21’	2.86	207.87	10955.65	13269.53
Aprill 21’	6.10	8.66	21356.67	521.96
ASL / ABL			**54845.28**	**27292.80**
TAL			**82.138**	

Table 3. Recording of suspended sediment (Cs) and bed (Cb) rates. Monthly suspended and bed loads (MSL and MBL), annual suspended and bed loads (ASL and ABL) and total annual load (TAL) for the period analysed.

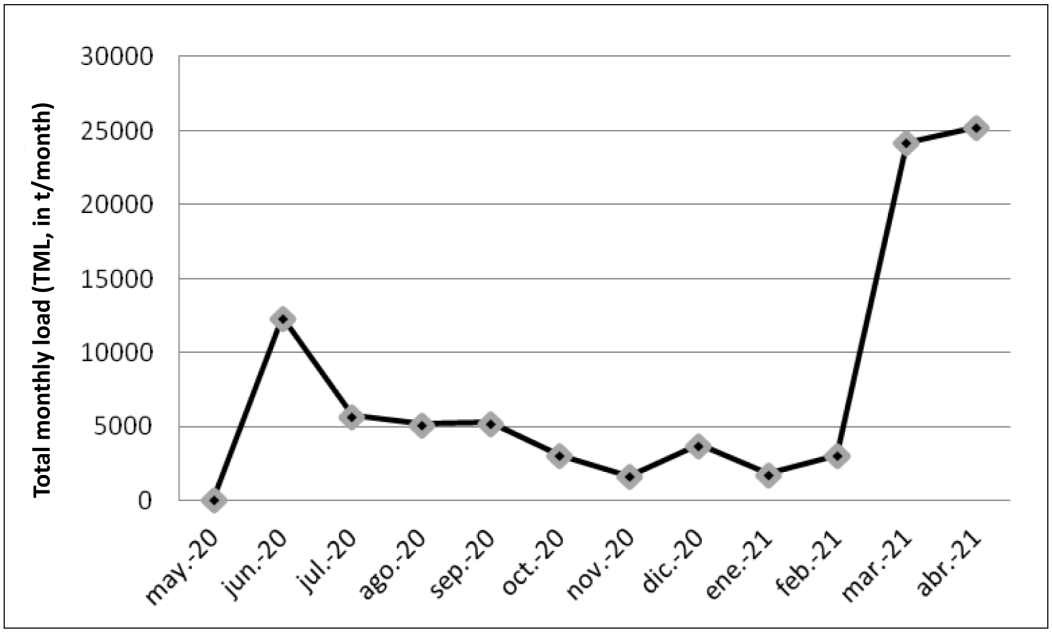

Figure 6. Total monthly load (TML, in t/month) originated in the basin of the period 2020/2021.

of the Rio Hondo reservoir, whose storage capacity was decreasing annually by 1.03% before the SFRB discharge (Mariot De Marco, 2001).

The quantified sediment transport values represent only 0.34% of the total erosion estimated by Bustos (2018) with the Revised Universal Soil Loss Equation (RUSLE) method (24.4 x 10^6 ton/yr). This difference is attributed to sediment retention in low topographic areas, the implementation of retention practices such the use of burlap bags in the channels, and nets in the fields, and/or the discharge of sediment from the channel through bifurcations/avulsions, primarily occurring during flood events (CEEH, 2018; Fig. 8). As a result, only a portion of the material produced

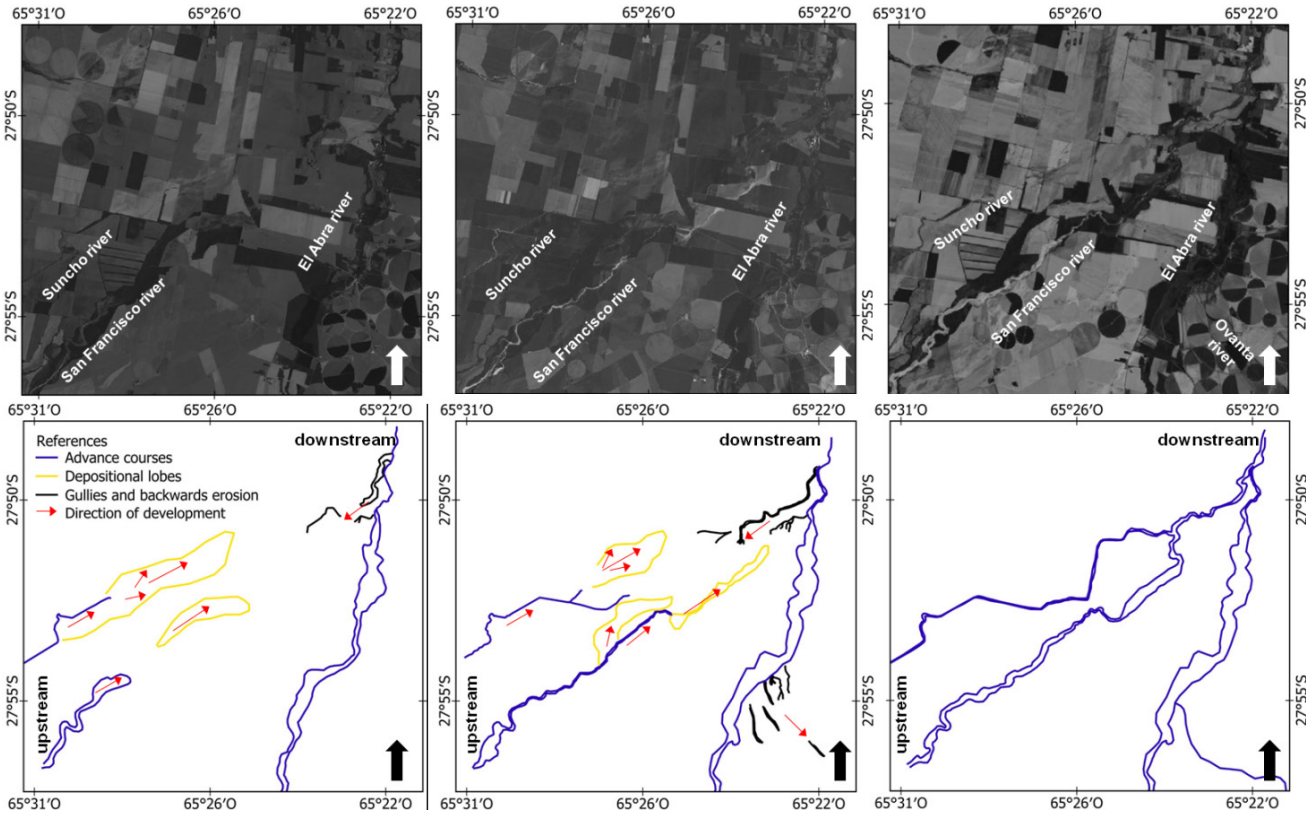

Figure 7. Main processes of development of the new drainage network. Formation progress is shown from left to right; in blue the formation of new channels by advancing depositional lobes (in yellow) and floodplain erosion; in black the development of gullies along the banks, scour and floodplain channelisation. The direction of development in both processes (upstream/downstream) is represented by red arrows.

by laminar erosion reaches the drainage network and the basin outlet. The simultaneous result of increased flow and sediment load is the expansion of channel width, meander wavelength, and the width-depth ratio (Schumm, 1977; Willis, 1989; Bridge, 1993; a detailed review in Bridge and Demicco, 2008).

In the SFRB, the lateral erosion processes became dominant when the drainage network was completely interconnected and shifted to a permanent regime. Figure 5 shows the trend to wider channels from upstream (Fig. 5a) to downstream (Fig. 5c). Even though in this study we only focussed on the progress of the drainage network and the amount of sediment and water delivered through the newly developed network, it is necessary to emphasize that both processes, enlargement and widening of the channels, were concomitant and are a direct result of the intensification of erosion processes linked spatially and temporally and enhanced by the anthropogenic changes produced in the basin.

The processes that acted together and could be documented on site during fieldwork, were piping in agricultural fields and roadsides (Fig. 9a and b), sapping in the riverbanks (Fig. 9c), gullies erosion and steep bank erosion ("barrancas"; Fig. 9d). Gullies were recorded in the areas of floodplain with gentle slopes where farmers deforested and ploughed the river margins. Another feature recorded in several sectors of all rivers are outcrops of Pleistocene (?) deposits in the margins or/and riverbed forming steps (Fig. 9e) as slope interruptions.

The original vegetation cover, the Chaqueño Forest, was reduced by deforestation to attend the agricultural expansion (CIST, 2017), which affected the flood and sedimentation buffering capacity of the wetland forests and riparian forests, resulting in reduced areas with vegetation in degraded condition (CEEH, 2018). In addition, rainfall records for the study area show an increase in more than 200 mm in mean annual precipitation since 1972 (Eremchuk *et al.*, 2016; Bazzano, 2019).

Along with the expansion of agriculture and livestock farming in the basin, water delivery was a key factor. In this way, the management techniques

of the excess water from centre-pivot irrigation systems and drain of wetlands are considered to be the triggers of intensified erosion (CEEH, 2018). Isuani (2024) indicates how excess water drains without the existence of natural barriers or elements that enhance the infiltration, energy dissipation, and sediment transport capacity in most of the watershed area. These are additional factors that intensify surface (laminar and streams) and subsurface (piping and sapping) erosion. Toledo *et al.* (2020), studying a nearby fluvial basin of SFRB, state that degradation processes in the catchment area, linked to inadequate management and overexploitation of cultivated soils, influenced the morphological changes of the rivers and the alteration of the physical properties of the soils increasing runoff and erosive processes on the riverbanks.

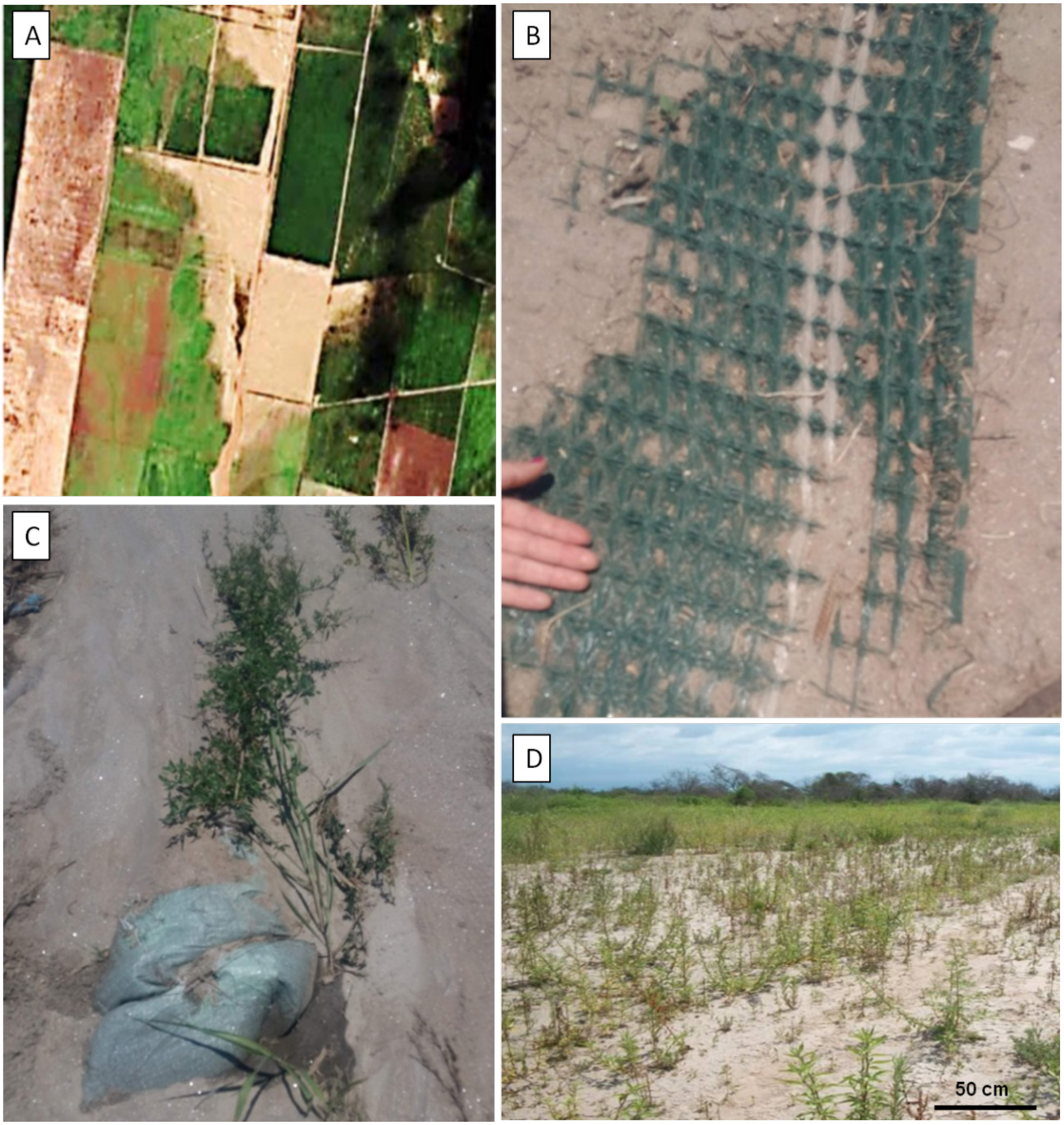

Figure 8. a) Sediment avulsion in the lower basin after extreme precipitation. **b)** Sediment retention netting in fields. **c)** Sediment retention pockets in the bed of the channel. d) Avulsion deposit in the lower basin.

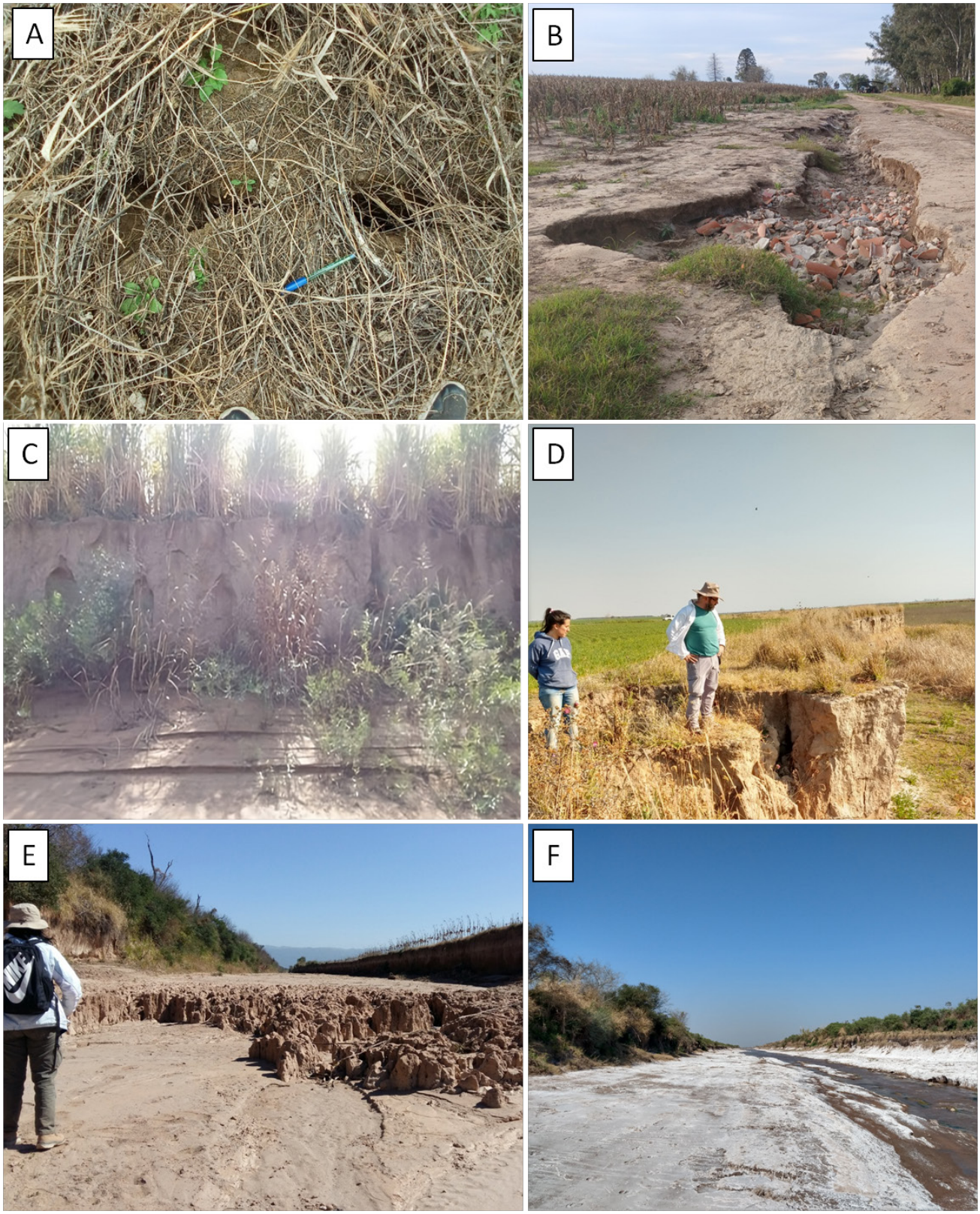

Figure 9. Erosion and salinisation processes documented in situ. **a)** Piping in agricultural fields. **b)** Gullies in roadside. **c)** Sapping in riverbank. **d)** Gully erosion and steep bank erosion. **e)** Pleistocene (?) deposits on the banks and/or riverbed forming steps. **f)** Salinisation in the lower part of the SFRB.

CONCLUSIONS AND SUGGESTIONS

Detailed processes analysis and data highlight the need for management in modified systems such as the San Francisco River Basin (SFRB). Anthropic activities (mainly the expansion of agricultural frontiers) in these sensitive areas, previously protected by natural native vegetation and wetlands, accelerated erosion and soil loss. This triggered in a few decades (between 1990 and 2018) the expansion and enlargement of the drainage network (more than 102 km of new channels), activating the delivery of sediment (82,132 ton/yr) and water (22 hm^3) through a new outlet connecting the SFRB and Marapa river basin, and doubling the catchment area at the confluence point (3,541 km^2). The excess of solid and liquid discharges delivered impact downstream accelerating siltation in the Rio Hondo reservoir.

The creation and implementation of a committee within interdepartmental and interprovincial systems is a crucial management measure. The articulation of criteria for the creation and regular updating of maps, along with the formulation and execution of initiatives in high-priority zones, is pivotal for addressing and responding to the impacts of both natural and human-induced changes in exceptionally productive watersheds (López and Patrón, 2013).

At present, given numerous studies carried out by government offices and scientific community on to the basin's problems, the SFRB is now being considered under the focus of and internationally scoped United Nations (UN) pilot project (SDG 6.6.1) aiming to develop a methodology for the restoration of freshwater ecosystems (UN Environment Programme, Action Plan, 2021).

Acknowledgments. The final version of this paper benefited from the comments of two anonymous reviewers and the associate editor Giorgio Basilici. The work was made possible thanks to the financial support of the Universidad Nacional de Tucumán (PIUNT G618) and a doctoral grant from Consejo Nacional de Investigaciones Científicas y Técnicas of Argentina to MAI.

REFERENCES

Aceñolaza, F. G., and Toselli, A. J. (1977). Esquema geológico de la Sierra de Ancasti, provincia de Catamarca. *Acta Geológica Lilloana*, 14, 233–259.

Aceñolaza, F. G., and Toselli, A. J. (1981). *Geología del Noroeste argentino*. Facultad Ciencias Naturales, Universidad Nacional de Tucumán, Publicación Especial 1287, 212 pp.

Aceñolaza, F. G., Durand, F., and Fernández, R. (1983). Fallas modernas. In F.G. Aceñolaza, H. Miller, and J. Toselli (Eds.), *La geología de la sierra de Ancasti* (pp. 243–251). Münster Forschungen zur Geologie und Palaontologie, Special Publication 59.

Azcuy Ameghino, E., and Ortega, L. E. (2010-12). *Sojización y expansión de la frontera agropecuaria en el NEA y NOA: transformaciones, problemas y debates* (Report No. 5, 141–159). Centro Interdisciplinario de Estudios Agrarios (CIEA), Facultad de Ciencias Económicas, Universidad de Buenos Aires.

Bakker, M. M., Govers, G., Kosmas, C., Vanacker, V., Van Oost, K., and Rounsevell, M. (2005). Soil erosion as a driver of land-use change. *Agriculture, ecosystems & environment*, 105(3), 467–481. https://doi.org/10.1016/j.agee.2004.07.009

Basile, P. A. (2018). *Transporte de sedimentos y morfodinámicas de ríos aluviales* (1st ed.). Editorial de la Universidad Nacional de Rosario, 455 pp.

Battaglia, A. A. C. (1982). *Carta geológico-económica de la República Argentina, provincias de Santiago del Estero, Catamarca y Tucumán, escala 1:200.000* (Boletín 186). Servicio Geológico Minero Argentino (SEGEMAR).

Bazzano, F. (2019). *Predicción de lluvias máximas para diseño hidrológico. Desarrollo experimental en la provincia de Tucumán* [Unpublished doctoral dissertation]. Universidad Nacional de Tucumán.

Blasco, G., Caminos, R. L., Lapido, O. R., Lizuaín, A., Martínez, H., Nullo, F. E., Panza, J. L. A., Sacomani, L. E., Barber, E. L. G., Chipulina, M. A., and Martínez, L. (1994). *Hoja Geológica 2966-II San Fernando del Valle de Catamarca, provincias de Catamarca, Santiago del Estero y Tucumán, escala 1:250.000* (Boletín 212). Instituto de Geología y Recursos Minerales, Servicio Geológico Minero Argentino (SEGEMAR).

Bridge, J. S. (1993). The interaction between channel geometry, water flow, sediment transport and deposition in braided rivers. In J. L. Best and C. S. Bristow (Eds.), *Braided Rivers* (pp. 13–71). Geological Society of London, Special Publication No. 75. https://doi.org/10.1144/GSL.SP.1993.075.01.02

Bridge, J., and Demicco, R. (2008). *Earth surface processes, landforms and sediment deposits*. Cambridge University Press.

Buono, N., Jobbágy, E., Nosetto, M., Menéndez, A., and Cáceres, R. (2018). *Aspectos hidrogeológicos en la formación abrupta de cursos fluviales en cuencas semiáridas sedimentarias* [Extended abstract]. XXVIII Congreso Latinoamericano de hidráulica, Buenos Aires Argentina. https://www.ina.gob.ar/congreso_hidraulica/resumenes/LADHI_2018_RE_465.pdf

Bustos, M. S. (2018). Estudio integral de procesos de erosión y sedimentación en la cuenca media del río San Francisco. In: *Estudio de los procesos dinámicos fluviales de erosión y sedimentación de los ríos San Francisco y Marapa y propuesta de medidas correctivas para la mitigación integral del riesgo de inundación en la zona de La madrid*. Final Technical Report (68 -77). Claudio Bravo Consultora: Proyecto (AR-L 1236).

Capolongo, D., Pennetta, L., Piccarreta, M., Fallacara, G., and Boenzi, F. (2008). Spatial and temporal variations in soil erosion and deposition due to land-levelling in a semi-arid area of Basilicata (Southern Italy). *Earth Surface Processes and Landforms*, 33(3), 364–379. https://doi.org/10.1002/esp.1560

Comisión Especial de Emergencia Hídrica (CEEH) (2018). *Plan Hídrico Estratégico de la Provincia de Tucumán, Estudio de la Cuenca Marapa-San Francisco*. Honorable Legislatura de Tucumán, Universidad Nacional de Tucumán. https://www.legislaturadetucuman.gob.ar/CEEH/pdfs/2CEEH-PHET-CRM-SF-Nov2018.pdf

Comisión de emergencia para el tratamiento de la problemática de inundaciones (CIST). (2017). *Problemática del área sur de Tucumán, este de Catamarca y Río Hondo* (Technical Report). Departamento Suelos, Dirección Flora, Fauna Silvestre y Suelos (SEMA) de Tucumán, Secretaría de Medio Ambiente de Tucumán, Dirección Nacional de Vialidad, Dirección Provincial de Vialidad de Tucumán, Dirección Provincial del Agua de Tucumán, Secretaría de Obras Públicas de Tucumán, Ejército Argentino, Universidad Nacional de Tucumán, Subsecretaría de Recursos Hídricos de la Nación, Secretaría de Medio Ambiente de Tucumán, Secretaría de Medio Ambiente de Tucumán, and Unidad Plan Belgrano de la Jefatura de Ministros del Gobierno Nacional. https://www.recursoshidricos.gov.ar/webdrh/_docs/CIST-Informe%20Completo.pdf

Coe, M. T., Latrubesse, E. M., Ferreira, M. E., and Amsler, M. L. (2011). The effects of deforestation and climate variability on the streamflow of the Araguaia River, Brazil. *Biogeochemistry*, 105, 119–131. https://doi.org/10.1007/s10533-011-9582-2

Contreras, S., Santoni, C. S., and Jobbágy, E. G. (2012). Abrupt watercourse formation in a semiarid sedimentary landscape of central Argentina: the roles of forest clearing, rainfall variability and seismic activity. *Ecohydrology*, 6(5), 794–805. https://doi.org/10.1002/eco.1302

Dal Molin, C. N., Fernández, D., and Escosteguy, L. D. (2003). *Hoja Geológica 2766-IV Concepción, Provincias de Tucumán, Catamarca y Santiago del Estero, escala 1:250.000* (Boletín 342). Servicio Geológico Minero Argentino (SEGEMAR).

Díaz Gómez, A. R. and Gaspari, F. J. (2017). Transformación territorial: Intensificación agraria y pérdida del suelo en la cuenca del río Marapa, Tucumán, Argentina. *Revista de la Facultad de Agronomía*, 116(2), 161–170.

El Esquiú, (2023, March 15). La lluvia provocó inundaciones en varias localidades del este catamarqueño. *El Esquiú*. https://www.elesquiu.com/sociedad/2023/3/15/la-lluvia-provoco-inundaciones-en-varias-localidades-del-este-catamarqueno-468952.html

Eremchuk, J., Cisternas, M. Y., and Costello, M. (2016). *Determinación de Áreas Inundables de las Localidades Ubicadas en la Cuencas de los Ríos El Abra, San Francisco, Ovanta y Las Cañas del Este Catamarqueño, Provincia de Catamarca* (Technical Report). Colegio de Geólogos de Catamarca.

Eremchuk, E. (2019). Geoamenazas por inundaciones de las geoformas fluviales de áreas urbanas y rurales de los principales ríos del centro y este de la provincia de Catamarca. *Revista de Geología Aplicada a la Ingeniería y al Ambiente*, 42, 35–47. https://biblat.unam.mx/hevila/Revistadegeologiaaplicadaalaingenieriayalambiente/2019/no42/4.pdf

González Bonorino, F. (1950). *Descripción Geológica de la Hoja 13e Villa Alberdi (Tucumán-Catamarca)* (Boletín 74). Dirección Nacional de Geología y Minería.

Guido, E. Y., Isuani, M. A., and Georgieff, S. M. (2022). *Cuencas hídricas de la provincia de Tucumán: actualización cartográfica* [Conference presentation abstract]. XXI Congreso Geológico Argentino, Puerto Madryn, Chubut. https://geologica.org.ar/xxi-cga-2022-chubut/

Isuani, M. A. (2024). *Hidrogeomorfología y Cuantificación de erosión y sedimentación de ríos de llanura: río San Francisco, Noroeste Argentino* [Unpublished doctoral dissertation]. Universidad Nacional de Tucumán.

La Gaceta (2017, April 3). El video de La Madrid desde adentro: el agua arrasó con todo y las calles se volvieron ríos. *La Gaceta*. https://www.lagaceta.com.ar/nota/724499/actualidad/video-madrid-desde-adentro-agua-arraso-todo-calles-se-volvieron-rios.html

López, R. F. P., and Patrón, E. R. (2013). *Cuencas hidrográficas. Fundamentos y perspectivas para su manejo y gestión*. Secretaría de Medio Ambiente y Recursos Naturales, México. https://biblioteca.semarnat.gob.mx/janium/Documentos/Ciga/Libros2013/Cuencas_final_2014.pdf

Lu, S., Jin, J., Zhou, J., Li, X., Ju, J., Li, M., Chen, F., Zhu, L., Zhao, H., Yan, Q., Xie, C., Yao, X., and Fagherazzi, S. (2021). Drainage basin reorganization and endorheic-exorheic transition triggered by climate change and human intervention. *Global and Planetary Change*, 201, Article 103494. https://doi.org/10.1016/j.gloplacha.2021.103494

Mariot De Marco, V. (2001). *Estudio de sedimentación del embalse de Río Hondo. Valoración cualitativa y cuantitativa de los problemas erosivos que afectan a la alta cuenca del río Salí-Dulce (provincias de Tucumán-Santiago del Estero, Argentina)* [Unpublished doctoral dissertation]. Universidad Politécnica de Madrid.

Mendoza, E. A., and González, J. A. (2011). Las ecorregiones del Noroeste Argentino: basadas en la clasificación climática de Köppen. In A. M. Frías de Fernández, B. Tracanna, and J. A. González (Eds.), *Serie Conservación de la Naturaleza* (pp. 3–41). Fundación Miguel Lillo, Publication 19. https://www.lillo.org.ar/revis/cnaturaleza/2011-scn-v19.pdf

Nullo, F. E. (1981). *Descripción Geológica de la Hoja 15 f, Huillapima, provincia de Catamarca, escala 1:200.000* (Boletín 178). Servicio Geológico Minero Argentino (SEGEMAR).

Pierce, S. C., Kröger, R., and Pezeshki, R. (2012). Managing artificially drained low-gradient agricultural headwaters for enhanced ecosystem functions. *Biology, 1*(3), 794-856. https://doi.org/10.3390/biology1030794

Schumm, S. A. (1977). *The Fluvial System*. John Wiley and Sons.

Toledo, M. A, Ahumada, A. L., and Ibañez Palacios, G. P. (2020). Alteraciones en el cauce del río Seco y pérdidas de tierras agrícolas, provincia de Tucumán, Argentina. *Boletín de la Sociedad Geológica Mexicana*, 72(2), Article 00012. https://doi.org/10.18268/bsgm2020v72n2a290719

Torrella, S., and Adámoli, J. (2005). Situación ambiental de la ecorregión del Chaco Seco. In A. Brown, U. Martinez Ortiz, M. Acerbi, and J. Corchera (Eds.), *La Situación Ambiental Argentina 2005* (pp. 75–82). Fundación Vida Silvestre Argentina. https://gran-chaco.agro.uba.ar/sites/default/files/pdf/sem2/FVSA-Ecorregi%C3%B3n%20Chaco%20Seco.pdf

Volante, J. N., Alcaraz-Segura, D., Mosciaro, M. J., Viglizzo, E. F., and Paruelo, J. M. (2012). Ecosystem functional changes associated with land clearing in NW. Argentina. *Agriculture,*

Ecosystems & Environment, 154, 12–22. https://doi.org/10.1016/j.agee.2011.08.012

Willis, B. J. (1989). Palaeochannel reconstructions from point bar deposits: a three-dimensional perspective. *Sedimentology, 36*(5), 757–766. https://doi.org/10.1111/j.1365-3091.1989.tb01744.x

Zheng, F. L. (2006). Effect of vegetation changes on soil erosion on the Loess Plateau. *Pedosphere, 16*(4), 420–427. https://doi.org/10.1016/S1002-0160(06)60071-4

Zilio, M. C., Aranda Alvarez, M. D. C., Zamponi, A., and Roggiero, M. (2022). Agriculturización y sapping en San Luis y Córdoba: señal antropocénica. In M. C. Zilio, G. M. D'Amico, and S. Báez (Eds.), *Volcán antropogénico. Una mirada geográfica sobre procesos geológicos y geomorfológicos* (pp. 258–271). Universidad Nacional de La Plata. https://www.memoria.fahce.unlp.edu.ar/libros/pm.5659/pm.5659.pdf